

# Clathrin and phosphatidylinositol-4,5-bisphosphate regulate autophagic lysosome reformation

Yueguang Rong<sup>1</sup>, Mei Liu<sup>1</sup>, Liang Ma<sup>1</sup>, Wanqing Du<sup>1</sup>, Hanshuo Zhang<sup>2</sup>, Yuan Tian<sup>3</sup>, Zhen Cao<sup>1</sup>, Ying Li<sup>4</sup>, He Ren<sup>5</sup>, Chuanmao Zhang<sup>5</sup>, Lin Li<sup>6</sup>, She Chen<sup>6</sup>, Jianzhong Xi<sup>2,7</sup> and Li Yu<sup>1,7</sup>

**Autophagy is a lysosome-based degradation pathway. During autophagy, lysosomes fuse with autophagosomes to form autolysosomes. Following starvation-induced autophagy, nascent lysosomes are formed from autolysosomal membranes through an evolutionarily conserved cellular process, autophagic lysosome reformation (ALR), which is critical for maintaining lysosome homeostasis. Here we report that clathrin and phosphatidylinositol-4,5-bisphosphate (PtdIns(4,5)P<sub>2</sub>) regulate ALR. Combining a screen of candidates identified through proteomic analysis of purified ALR tubules, and large-scale RNAi knockdown, we unveiled a tightly regulated molecular pathway that controls lysosome homeostasis, in which clathrin and PtdIns(4,5)P<sub>2</sub> are the central components. Our functional study demonstrates the central role of clathrin and its associated proteins in cargo sorting, phospholipid conversion, initiation of autolysosome tubulation, and proto-lysosome budding during ALR. Our data not only uncover a molecular pathway by which lysosome homeostasis is maintained through the ALR process, but also reveal unexpected functions of clathrin and PtdIns(4,5)P<sub>2</sub> in lysosome homeostasis.**

Autophagy is an evolutionarily conserved, lysosome-based degradation pathway<sup>1</sup>. Starvation leads to the deactivation of the mammalian target of rapamycin (mTOR), a master regulator of autophagy, which triggers the formation of double-membrane autophagosomes<sup>2,3</sup>. Multiple lysosomes fuse with an autophagosome to form an autolysosome, where sequestered cellular contents are degraded. Degradation products such as amino acids and sugars are released into the cytosol from autolysosomes through lysosome efflux transporters<sup>4</sup>. The release of nutrients from autolysosomes reactivates mTOR, triggering the termination of autophagy and the formation of nascent lysosomes from autophagic membranes, a process termed ALR (ref. 5). During ALR, tubular structures named reformation tubules extrude from autolysosomes. Small proto-lysosomes eventually pinch off from the reformation tubules. Proto-lysosomes contain autolysosomal membrane components, but lack components from autophagosomes. After a maturation process, proto-lysosomes acquire acidity and degradation capacity and become functional lysosomes<sup>5</sup>.

ALR is a complicated cellular process that probably requires sophisticated molecular machinery, but little is known about the governing mechanisms. Recently we found that the lysosomal efflux transporter Spinster is essential for initiating<sup>6</sup> ALR. Here we identified a

clathrin- and phosphatidylinositol-4,5-bisphosphate-based mechanism that plays a central role in regulating ALR.

## RESULTS

### Systematic identification of proteins required for ALR

To identify proteins required for ALR in a systematic manner, we took a combined approach that included proteomic analysis, large-scale RNA-mediated interference (RNAi) screening and functional studies (Fig. 1a). Proteins present on reformation tubules were first identified by proteomic analysis of purified ALR tubules. Their involvement in ALR was then tested using RNAi screening, and the specific roles of the identified proteins in ALR were determined by functional studies.

First, we purified reformation tubules from NRK cells through a purification protocol developed previously<sup>5</sup>. Our purification protocol yielded LC3- and LAMP2-positive tubules with relatively high purity (Fig. 1b). Independent mass spectrometry analyses were carried out on reformation tubules from three separate purifications. Details of the mass spectrometry analysis and database searching are shown in Supplementary Table S1. Of the 2,225 proteins identified in total from these three experiments (Supplementary Table S2), 29.3% were identified in all three experiments and 46.3% were identified in at

<sup>1</sup>State Key Laboratory of Biomembrane and Membrane Biotechnology, Tsinghua University-Peking University Center for Life Sciences, School of Life Science, Tsinghua University, Beijing 100084, China. <sup>2</sup>College of Engineering, Peking University, Beijing 100871, China. <sup>3</sup>College of Biological Sciences, China Agricultural University, Beijing 100193, China. <sup>4</sup>Cell Biology Core Facility, Tsinghua University, Beijing 100084, China. <sup>5</sup>School of Life Sciences, Peking University, Beijing 100871, China.

<sup>6</sup>Proteomics Facility, National Institute of Biological Sciences, Beijing 102206, China.

<sup>7</sup>Correspondence should be addressed to J.X. or L.Y. (e-mail: jxzi@pku.edu.cn or liyulab@mail.tsinghua.edu.cn)

Received 14 May 2012; accepted 9 July 2012; published online 12 August 2012; DOI: 10.1038/ncb2557

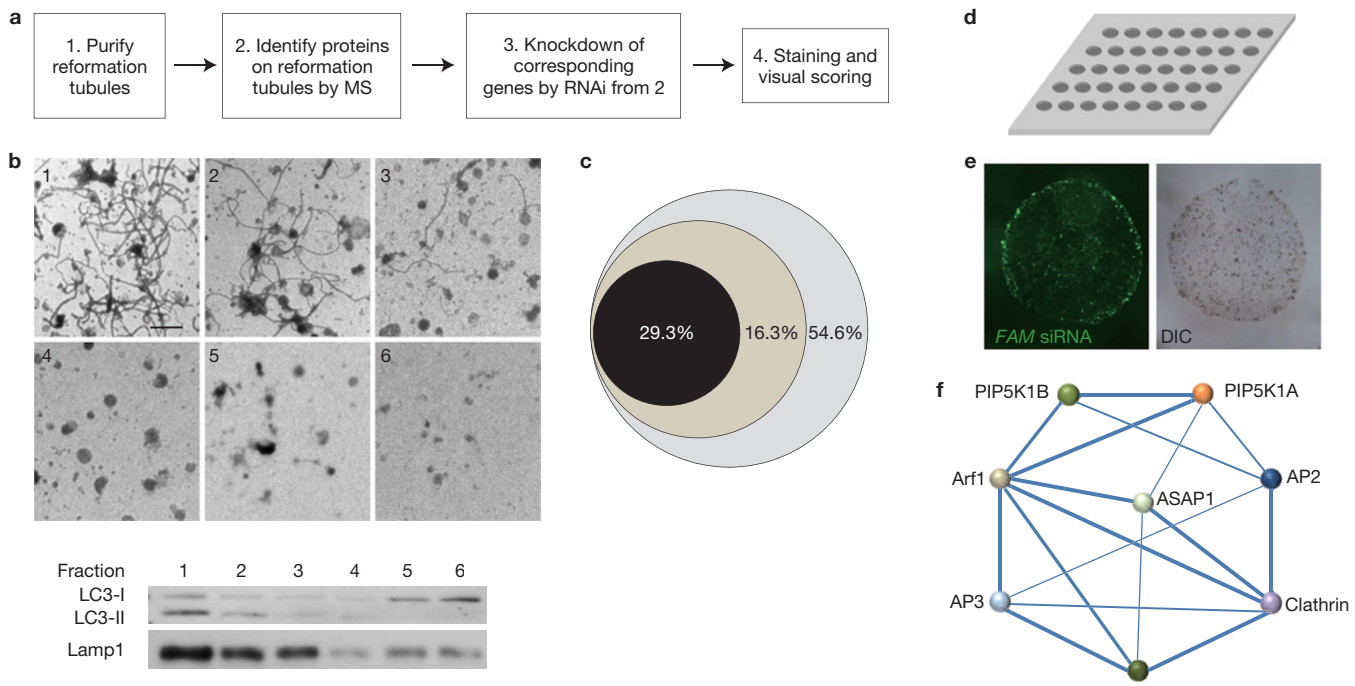


**Figure 1** Identification of genes regulating ALR by proteomic analysis and SAMCell-RNAi screening. **(a)** Outline of the screening strategy. MS, mass spectrometry. See the text for details. **(b)** Density gradient fractions of NRK cells starved for 8 h were analysed by transmission electron microscopy (upper panel) and blotted for LC3 or LAMP2 (lower panel). Proteins in fraction 1 were identified by mass spectrometric analysis. Three replicates were carried out from three independent purifications. Scale bar, 2  $\mu$ m. **(c)** The dark grey circle shows the percentage of proteins identified from all three purifications; the grey circle shows the percentage of proteins

identified from two of the three experiments. **(d)** Diagram of a SAMCell. Each dot represents a self-assembled cell island that can be transfected with an individual RNAi. **(e)** NRK cells grown on the SAMCell were transfected with *FAM*-RNAi by reverse transfection and the transfection efficiency was monitored by microscopy. Left panel, *FAM*-RNAi-positive cells; right panel, differential interference contrast (DIC) image of the cells in the left panel. **(f)** Functional associations were analysed by STRING. Stronger associations are represented by thicker lines. Uncropped images of blots are shown in Supplementary Fig. S6.

least two experiments (Fig. 1c). We picked 114 proteins as our primary targets for further analysis on the basis of their membrane localization or their known function in membrane trafficking and vesicle formation (Supplementary Table S3).

Next, we screened our primary targets for a role in ALR by RNAi knockdown. We previously showed that blocking of ALR leads to the arrest of autophagy at the autolysosomal stage, resulting in the accumulation of large, persistent, LC3-positive autolysosomes<sup>5</sup>. Autolysosomes can be easily identified through staining with LC3, so we used LC3 staining as the screening marker. As ALR is triggered by mTOR reactivation and mTOR knockdown has been shown to block ALR (ref. 5), we used *mTOR*-RNAi as our positive control.

We carried out the screen using a recently developed method, SAMCell, which allows the delivery of a large number of individual RNAi molecules to cell islands grown on single glass slides with high efficiency (Fig. 1d,e)<sup>7</sup>. We starved RNAi-treated NRK cells for 12 h, after which time autophagy is largely terminated and there are almost no LC3-positive autolysosomes in nonspecific-RNAi-transfected cells. RNAi treatments causing accumulation of large LC3-positive punctate structures in starved cells were identified as candidate genes for further study (Supplementary Fig. S1). By this method, we obtained *Cltc* (clathrin heavy chain), *Arf1* and *PIP5K1A*, with a potential role in ALR. We also screened genes encoding proteins that are physically or functionally associated with the protein products of these candidate

genes, and identified *AP2*, *AP3*, *AP4* and *PIP5K1B*, *ASAP1* as potential regulators of ALR. These proteins were analysed using the Search Tool for the Retrieval of Interacting Genes/Proteins (STRING), which predicted a strong functional association among them (Fig. 1f).

### Clathrin regulates ALR

We investigated a role for clathrin in ALR by RNAi knockdown of the clathrin heavy chain gene (*Cltc*) using a standard RNAi protocol in NRK cells that stably express LC3–CFP and LAMP1–YFP (Supplementary Fig. S2a). In most *Cltc* knockdown cells, we observed large, LC3/LAMP1-positive autolysosomes 12 h after starvation, whereas in nonspecific RNAi-transfected cells, most autolysosomes did not persist (Fig. 2a,b). Transmission electron microscopy (TEM) analysis verified the massive accumulation of autolysosomes in *Cltc* knockdown cells (Fig. 2c). These results indicate that clathrin is required for ALR.

Clathrin plays a major role in the formation of coated vesicles<sup>8,9</sup>. Clathrin-coated vesicles sort cargos from different membrane compartments, including the plasma membrane and the *trans*-Golgi network<sup>10</sup>. Apart from its role in vesicle formation, clathrin has also been reported to regulate the segregation of cargo and the generation of different domains on endosomal membranes<sup>11</sup>, and the sorting of cargo from endosomes to the Golgi<sup>12,13</sup>.

To investigate whether clathrin directly regulates ALR, we investigated whether or not clathrin is present on autolysosomes.

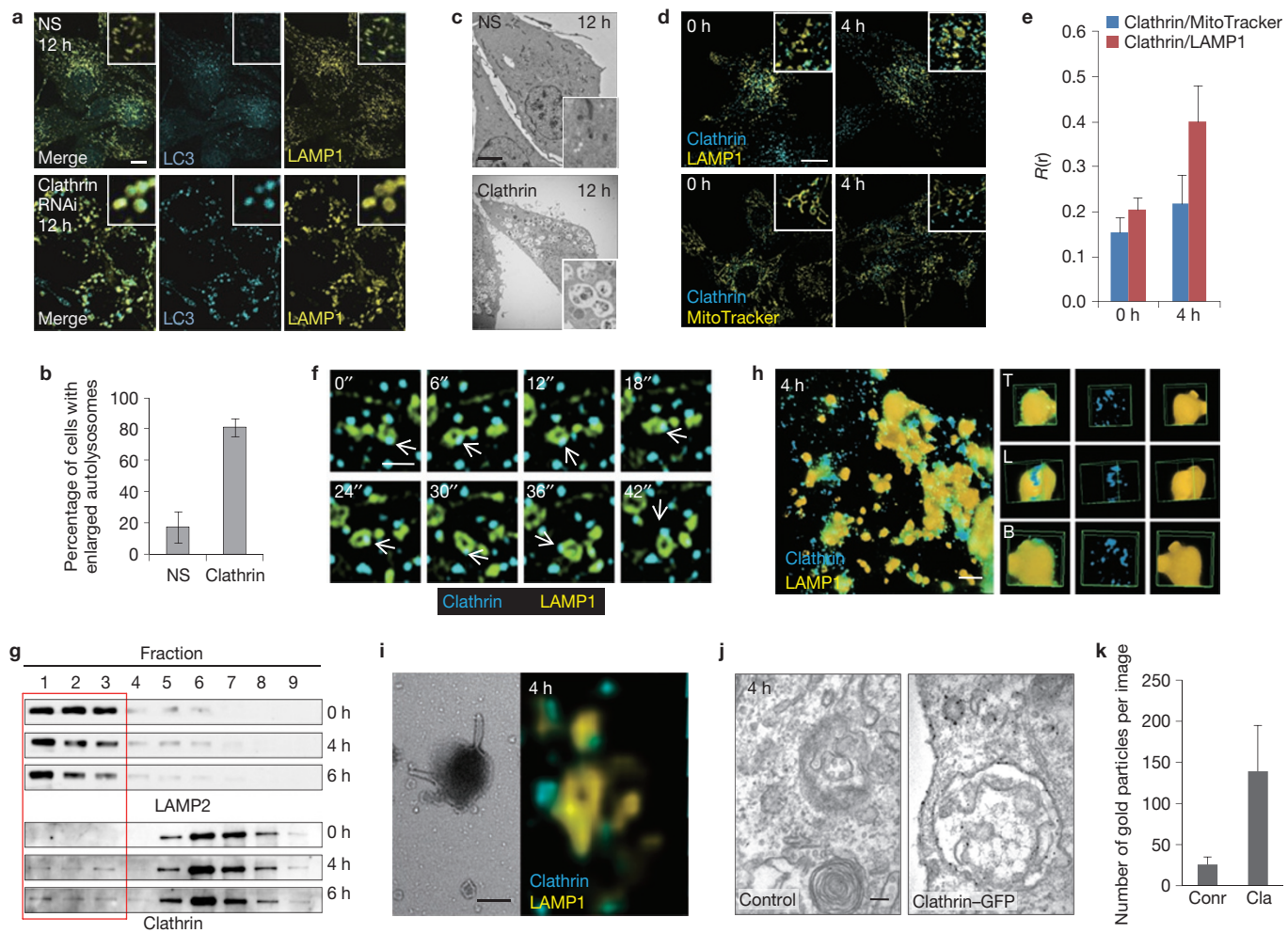


**Figure 2** Clathrin regulates ALR. **(a)** NRK cells stably expressing CFP–LC3; LAMP1–YFP were transfected with nonspecific (NS)- or *Cltc* (clathrin heavy chain)-RNAi and starved for 12 h. Scale bar, 5 µm. **(b)** Cells from **a** were assessed for enlarged autolysosomes after starvation and quantified.  $n = 100$  cells from three independent experiments. Error bars indicate the s.d. **(c)** Representative TEM micrographs of nonspecific- or *Cltc*-RNAi-transfected NRK cells after 12 h of serum starvation. Scale bar, 5 µm. **(d)** NRK cell lines stably expressing LAMP1–Cherry; clathrin–GFP were starved for 0 or 4 h and observed by confocal microscopy. As a control, clathrin–GFP-expressing cells were starved for 0 or 4 h and then stained with MitoTracker red. Scale bar, 5 µm. The insets in **a**, **c** and **d** represent enlarged regions of interest. **(e)** Cells from **d** were analysed for Pearson's co-localization coefficient ( $R(r)$ ).  $n = 30$  cells from three independent experiments. Error bars indicate the s.d. **(f)** NRK cells stably expressing LAMP1–Cherry; clathrin–GFP were starved for 4 h and time-lapse images were acquired by spinning-disc microscopy. Scale bar, 500 nm. The white arrows indicate a clathrin punctum moving along a LAMP1-positive

We first established a stable cell line expressing clathrin light chain fused to GFP (clathrin–GFP) and LAMP1–Cherry at low levels. We analysed the co-localization of clathrin–GFP and LAMP1–Cherry before and after starvation. As starvation can cause cells to round up, to rule out the possibility that any change in co-localization is an artefact due to a starvation-induced shape change, we used the co-localization of clathrin–GFP and LAMP1–Cherry markedly increased after starvation, whereas the co-localization of MitoTracker

structure. **(g)** NRK cells were starved for 0, 4 or 6 h and then subjected to cell fractionation. Fractions were analysed by western blotting with antibodies against LAMP2 and clathrin heavy chain. 1 is the top fraction. The outline indicates the Lamp2-positive fraction. **(h)** Cell lines stably expressing clathrin–GFP were starved for 4 h, stained with antibodies against GFP and LAMP1, analysed by 3D-SIM. Scale bar, 2.5 µm. The right panels show enlarged regions of interest from the left panel: T, top view; L, lateral view; B, bottom view. **(i)** Left panel, representative TEM micrographs of purified autolysosomes from starved clathrin–GFP-expressing cells. Scale bar, 250 nm. Right panel, SIM image of purified autolysosomes stained with GFP and LAMP1 from the same experiment. Scale bar, 5 µm. **(j)** NRK or stable clathrin–GFP-expressing NRK cell lines were analysed by pre-embedding-immuno-electron microscopy using antibodies against GFP. Scale bar, 100 nm. **(k)** Quantification of the average number of gold particles per image from control or clathrin–GFP cells.  $n = 25$  images from three independent experiments. The error bars indicate the s.d. Uncropped images of blots are shown in Supplementary Fig. S6.

and clathrin only marginally increased (Fig. 2d,e). Thus, we concluded that the increasing co-localization of clathrin and LAMP1 probably resulted from increasing recruitment of clathrin. As clathrin has many sites of action within cells, and LAMP1-positive vesicles are widely distributed, the overlapping signals may reflect coincidental overlap of other clathrin-containing structures with autolysosomes rather than real co-localization of clathrin and LAMP1. To rule out this possibility, we carried out time-lapse imaging of LAMP1 and clathrin, and found that some clathrin puncta moved along with the LAMP1–Cherry-

positive structures (Fig. 2f), suggesting that at least some co-localization reflects the presence of clathrin on autolysosomes. Furthermore, we performed cellular fractionation and analysed the presence of clathrin in autolysosomes. We found that almost no clathrin is co-fractionated with LAMP2 before starvation; however, after 4 h starvation, a small amount of clathrin is present in the autolysosome fraction (Fig. 2g). To investigate how clathrin is localized on autolysosomes, we stained intact cells or purified autolysosomes with antibodies against clathrin and LAMP1, and analysed these samples using three-dimensional structured illumination microscopy (3D-SIM). We found that clathrin is present on the surface of autolysosomes in the form of small buds, and most of these clathrin-positive buds are closely associated with, and embedded into, autolysosomes (Fig. 2h,i). We also performed pre-embedding-immuno-electron microscopy analysis in clathrin-GFP-expressing cells using an antibody against GFP, and found that clathrin is present on autolysosomes (Fig. 2j,k). Putting all of these data together, we concluded that clathrin is recruited to autolysosomes during ALR. Thus, it is possible that clathrin regulates ALR directly.

#### PtdIns(4,5)P<sub>2</sub> and PIP5K1B are required for ALR

Phosphoinositide is an important signalling molecule that defines the identity of intracellular membrane systems<sup>14</sup>. Phosphoinositide operates in two different ways. First, on stimulation, phosphoinositide can be produced rapidly and in a highly localized manner to convey spatial and temporal information about a particular cellular event<sup>15</sup>. Second, specific phosphoinositides exhibit a steady-state enrichment in specific organelles; they function as organelle-specific platforms to recruit phosphoinositide-binding proteins and therefore create distinguishing features of organelle membranes<sup>16</sup>.

Our screen identified phosphatidylinositol-4-phosphate 5-kinase (PIP5K1B) as a candidate for regulating ALR. PtdIns(4,5)P<sub>2</sub> is synthesized from PI(4)P by phosphatidylinositol-4-phosphate 5-kinase<sup>17,18</sup> including PIP5K1B. Knockdown of *PIP5K1B* led to the inhibition of ALR, resulting in the formation of long-lasting LC3–CFP- and LAMP1–YFP-positive autolysosomes after starvation (Fig. 3a–c and Supplementary Fig. S2). These data suggested that PIP5K1B and PtdIns(4,5)P<sub>2</sub> may play an essential role in extrusion of reformation tubules.

Next, we examined the localization of PIP5K1B. 3D-SIM revealed that PIP5K1B forms small puncta within the cell, some of which decorate autolysosomes (Fig. 3d). Cellular fractionation also revealed a small amount of PIP5K1B on autolysosomes (Fig. 3e). These data suggested that PIP5K1B converts PI(4)P into PtdIns(4,5)P<sub>2</sub> on autolysosomes.

As it is well established that PtdIns(4,5)P<sub>2</sub> is required for recruiting clathrin to membranes<sup>19</sup>, we next examined the localization of PtdIns(4,5)P<sub>2</sub> on autolysosomes. We stained purified, structurally intact autolysosomes (Fig. 3f, left panel) using antibodies against PI(4)P, PtdIns(4,5)P<sub>2</sub> and LAMP1. We found that PI(4)P was present on autolysosomes, and almost perfectly co-localized with LAMP1, indicating that PI(4)P is ubiquitous on autolysosomes (Fig. 3f). We also detected the presence of PtdIns(4,5)P<sub>2</sub> on autolysosomes. Interestingly, we found that PtdIns(4,5)P<sub>2</sub> is highly enriched on autolysosome buds, with very little or none on the main autolysosome body (Fig. 3f).

To investigate the distribution of PI(4)P during autophagy, we stained cells with an antibody against PI(4)P and found that PI(4)P

is present on perinuclear Golgi-like structures before starvation, but becomes more diffusely localized 4 h after starvation (Fig. 3g). To better study the dynamics of PI(4)P localization, we established a cell line that stably expresses OSBP-PH-GFP, a widely used PI(4)P probe<sup>20,21</sup>, and LAMP1-Cherry. We found that OSBP-PH-GFP is exclusively present on the Golgi under normal growth conditions. However, after 4 h of starvation, much of the OSBP-PH-GFP is present on autolysosomes, whereas 8 h after starvation, OSBP-PH-GFP has a dispersed localization pattern again (Fig. 3h). As PIP5K1B converts PI(4)P into PtdIns(4,5)P<sub>2</sub>, we investigated whether knockdown of *PIP5K1B* affects the distribution of PI(4)P. We found that after 12 h of starvation, very little OSBP-PH-GFP is present on nascent lysosomes, whereas in *PIP5K1B* knockdown cells, OSBP-PH-GFP accumulates on enlarged autolysosomes (Fig. 3i), implying that knockdown of *PIP5K1B* may affect the conversion of PI(4)P to PtdIns(4,5)P<sub>2</sub> on autolysosomes. Furthermore, we found that *PIP5K1B* knockdown leads to a change in the clathrin localization pattern and a reduction in the level of co-localization of clathrin and autolysosomes (Fig. 3j,k). These data suggest that PtdIns(4,5)P<sub>2</sub> and PIP5K1B play an essential role in ALR by regulating the recruitment of clathrin.

#### PIP5K1A is required for proto-lysosomes to pinch off from reformation tubules

Besides *PIP5K1B*, we also identified *PIP5K1A* in our RNAi screen. PIP5K1A and PIP5K1B are encoded by two different genes that share 68% sequence identity<sup>17</sup>. In a small subset of cells, *PIP5K1A* knockdown led to the formation of enlarged autolysosomes with a reduced number of reformation tubules; in most cells, knockdown of *PIP5K1A* caused marked elongation and stabilization of reformation tubules (Fig. 4a–c and Supplementary Fig. S2). We also found that the elongation of reformation tubules is accompanied by a reduction in the number of proto-lysosomes/lysosomes. Interestingly, these elongated tubules are also more smooth, with fewer buds.

Reformation tubules are composed of a round or oval-shaped head and a long tubular tail (Fig. 4d). We found that in *PIP5K1A* knockdown cells, the ratio between the length of the tail (L) and the radius of the ‘head’ (R) is significantly increased (Fig. 4d–f). As the total membrane surface of autolysosomes is constant during tubule elongation, the elongation of a tail should accompany the reduction of head size. An increase in L/R indicates that reformation tubules can be successfully initiated and extended, and that the elongated reformation tubules in *PIP5K1A* knockdown cells most likely result from a defective fission/budding step.

The requirement of PIP5K1A for fission of proto-lysosomes suggests the possibility that PtdIns(4,5)P<sub>2</sub> is required for the fission step. To directly visualize the presence of PtdIns(4,5)P<sub>2</sub> in reformation tubules, we stained purified reformation tubules with an antibody against PtdIns(4,5)P<sub>2</sub>. We found that PtdIns(4,5)P<sub>2</sub> is enriched on the buds and tips of reformation tubules whereas PI(4)P is ubiquitously distributed on autolysosomes (Fig. 4g). We also found that PIP5K1A is localized to the tips and buds of the tubules (Fig. 4h). Cellular fractionation also revealed the presence of PIP5K1A on autolysosomes (Fig. 4i). Taken together, these data indicate that PIP5K1A may convert PI(4)P to PtdIns(4,5)P<sub>2</sub> on reformation tubules, thus initiating the fission/budding of proto-lysosomes from reformation tubules.

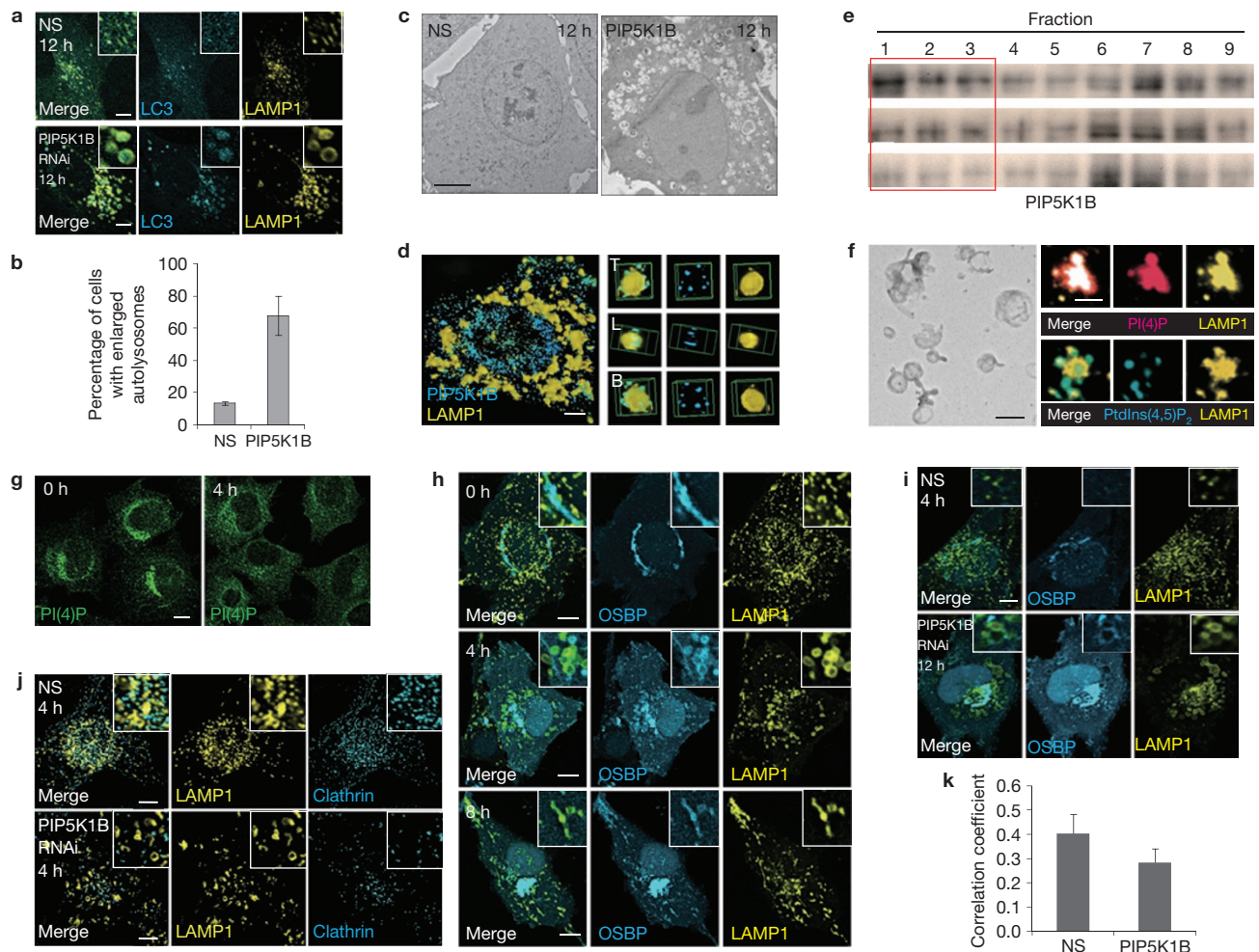


**Figure 3** PIP5K1B is required for the initiation of ALR. (a) NRK cell lines stably expressing CFP-LC3; LAMP1-YFP were transfected with nonspecific (NS)- or *PIP5K1B*-RNAi and starved for 12 h. Scale bars, 5  $\mu$ m. (b) Cells from a were assessed for enlarged autolysosomes in a blind fashion after starvation and quantified.  $n = 100$  cells from three independent experiments. Error bars indicate the s.d. (c) Representative TEM micrographs of nonspecific- or *PIP5K1B*-RNAi-transfected NRK cells after 12 h of serum starvation. Scale bar, 5  $\mu$ m. (d) NRK cells were starved for 4 h, stained with antibodies against PIP5K1B and LAMP1, and then analysed by 3D-SIM. Scale bar, 2.5  $\mu$ m. The right panels show enlarged regions of interest from the left panel: T, top view; L, lateral view; B, bottom view. (e) Fractions from Fig. 2f were analysed by western blotting with an antibody against PIP5K1B. The outline indicates the LAMP2-positive fraction. (f) NRK cells were starved for 4 h, autolysosomes were purified by density fractionation (left panel), and the quality of purified autolysosomes was monitored by TEM (left panel).

#### Clathrin is required for budding of proto-lysosomes from reformation tubules

We previously reported that proto-lysosomes pinch off from the tips of reformation tubules<sup>5</sup>. We also observed budding of proto-lysosomes from the middle of reformation tubules (Fig. 4j). The requirement of PtdIns(4,5)P<sub>2</sub> for proto-lysosome budding prompted us to investigate whether clathrin plays a role in this process. We found that after 8 h of starvation, many clathrin-GFP puncta localize to the tips of reformation tubules (Fig. 4k). As PtdIns(4,5)P<sub>2</sub> is required to recruit clathrin to membranes, we reasoned that the elongation of reformation tubules could result from reduced

Right panel, purified autolysosomes stained with antibodies against PI(4)P and PtdIns(4,5)P<sub>2</sub>. Scale bar, 500 nm. (g) NRK cells were starved for 0 or 4 h and stained with antibody against PI(4)P. Scale bar, 5  $\mu$ m. (h) NRK cells lines stably expressing OSBP-PH-GFP;LAMP1-Cherry were starved for 0, 4, or 8 h and observed by confocal microscopy. Scale bars, 5  $\mu$ m. (i) NRK cell lines stably expressing OSBP-PH-GFP;LAMP1-Cherry were transfected with *PIP5K1B*-RNAi. At 60 h after transfection, cells were starved for 12 h and analysed by confocal microscopy. Scale bar, 5  $\mu$ m. (j) NRK cell lines stably expressing LAMP1-Cherry;clathrin-GFP were transfected with nonspecific- or *PIP5K1B*-RNAi and starved for 12 h, and then observed by confocal microscopy. Scale bars, 5  $\mu$ m. The insets in a, h–j represent enlarged regions of interest. (k) Cells from g were analysed for Pearson's co-localization coefficient ( $R(r)$ ) by Olympus Fluoview.  $n = 30$  cells from three independent experiments. Error bars indicate the s.d. Uncropped images of blots are shown in Supplementary Fig. S6.

clathrin recruitment. To test this hypothesis, we knocked down *PIP5K1A* in clathrin-GFP/LAMP1-Cherry cells and analysed the number of clathrin-GFP puncta associated with reformation tubules. We found that the average distance between two clathrin-GFP dots on reformation tubules is significantly increased in *PIP5K1A* knockdown cells (Fig. 4l,m). These data indicate that *PIP5K1A* knockdown significantly reduces the number of clathrin-GFP puncta on reformation tubules. We concluded that *PIP5K1A* regulates the fission of proto-lysosomes, most probably through a clathrin-dependent mechanism. Taking all the data together, we speculated that clathrin may have two sites of action in ALR, one on autophagosomes,

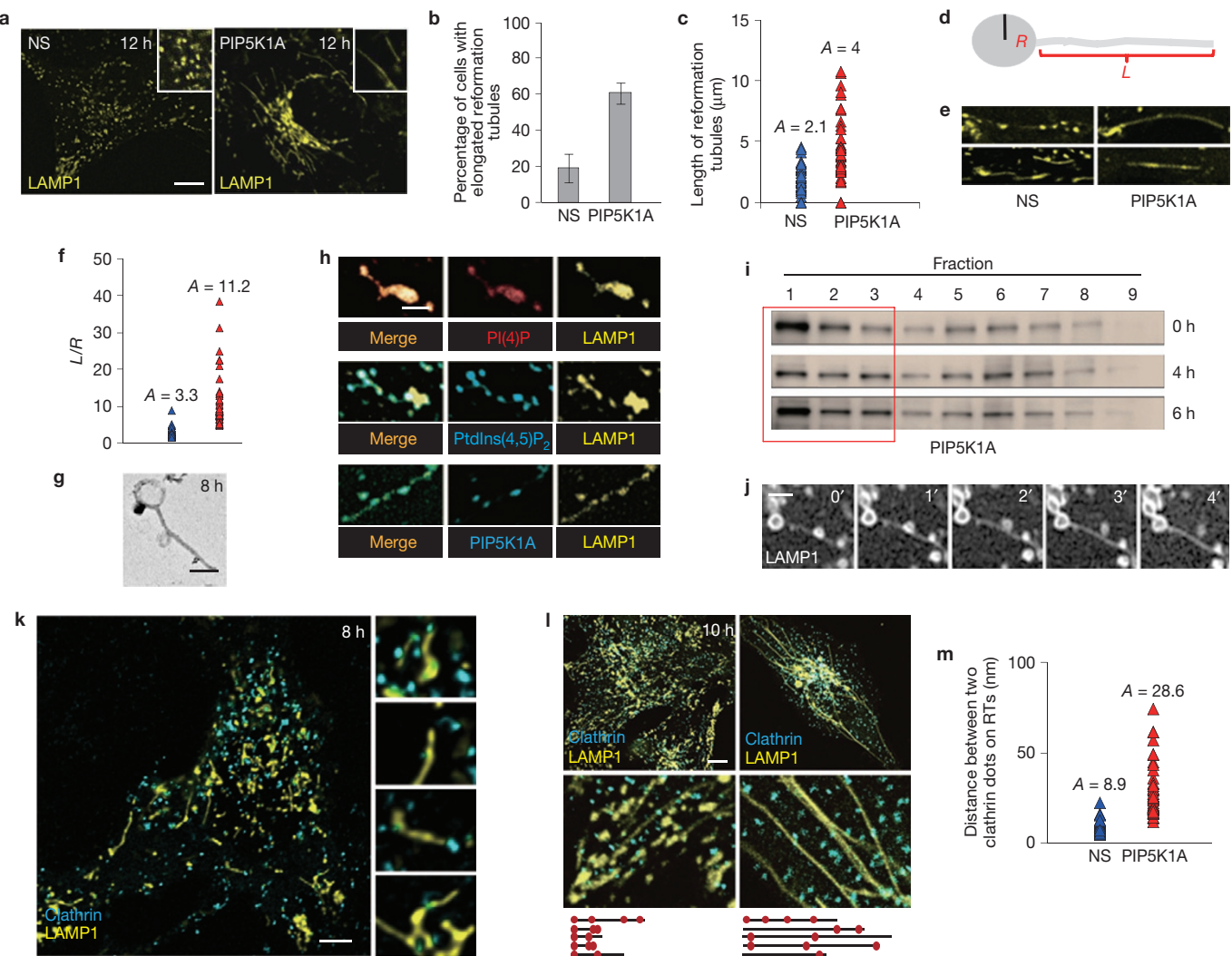


**Figure 4** Phosphatidylinositol-4-phosphate 5-kinase (PIP5K1A) is required for proto-lysosome budding during ALR. **(a)** NRK cells stably expressing CFP-LC3;LAMP1-YFP were transfected with nonspecific (NS)- or PIP5K1A-RNAi and starved for 10 h. The insets represent enlarged regions of interest. Scale bar, 5 μm. **(b)** Cells from **a** were assessed for the presence of elongated reformation tubules in a blind fashion after starvation and quantified.  $n = 100$  cells from three independent experiments. Error bars indicate the s.d. **(c)** Cells from **a** were assessed for the length of reformation tubules in a blind fashion after starvation and quantified. 50 cells were counted. The average tubule length is indicated above each column. **(d)** Diagram of reformation tubules.  $R$ , radius of main body;  $L$ , length. **(e)** Representative image of reformation tubules in nonspecific- or PIP5K1A-RNAi-transfected cells. The top and bottom panels show two randomly selected images of the respective samples. **(f)** Cells from **a** were assessed for the  $L/R$  ratio of reformation tubules in a blind fashion after starvation and quantified. 25 cells were counted. The average  $L/R$  is indicated above each column. **(g)** Purified reformation tubules were monitored by TEM. Scale bar, 250 nm. **(h)** Purified reformation tubules

stained with antibodies against PI(4)P, PtdIns(4,5)P<sub>2</sub> and PIP5K1A. Scale bar, 250 nm. **(i)** Fractions from Fig. 2f were analysed by western blotting with an antibody against PIP5K1A. The outline indicates the LAMP2-positive fraction. **(j)** NRK cells stably expressing CFP-LC3;LAMP1-YFP were starved for 8 h, and the budding of proto-lysosomes was monitored by spinning-disc microscopy. Scale bar, 100 nm. **(k)** NRK cell lines stably expressing LAMP1-Cherry;clathrin-GFP were starved for 8 h and observed by confocal microscopy. The right panels show enlarged regions of interest. Scale bar, 5 μm. **(l)** NRK cell lines stably expressing LAMP1-Cherry;clathrin-GFP were transfected with nonspecific- or PIP5K1A-RNAi and starved for 8 h. Scale bar, 5 μm. The middle panels show enlarged regions of interest from the upper panels. The distance between clathrin dots in the upper panels is shown in diagrammatic form in the lower panels. Black line: reformation tubules; red dot: clathrin. **(m)** The distance between two clathrin dots on reformation tubules (RTs) in cells from **l** was accessed in a blind fashion. Twenty-five cells were counted. The average distance between two clathrin dots is indicated above each column. Uncropped images of blots are shown in Supplementary Fig. S6.

where it is required for tubule initiation, and another on reformation tubules, where it is required for budding of proto-lysosomes.

### AP2 regulates ALR

It is well established that adaptor protein 2 (AP2) links clathrin with PtdIns(4,5)P<sub>2</sub> (refs 22,23). We found that AP2 knockdown blocks

ALR and leads to the accumulation of enlarged autolysosomes after 12 h of starvation (Fig. 5a–c and Supplementary Fig. S2). 3D-SIM revealed decoration of autolysosomes by small AP2 puncta (Fig. 5d) and cellular fractionation showed increasing recruitment of AP2 to autolysosomes after starvation (Fig. 5e), indicating that AP2 is recruited to autolysosomes during autophagy. To determine whether AP2 is

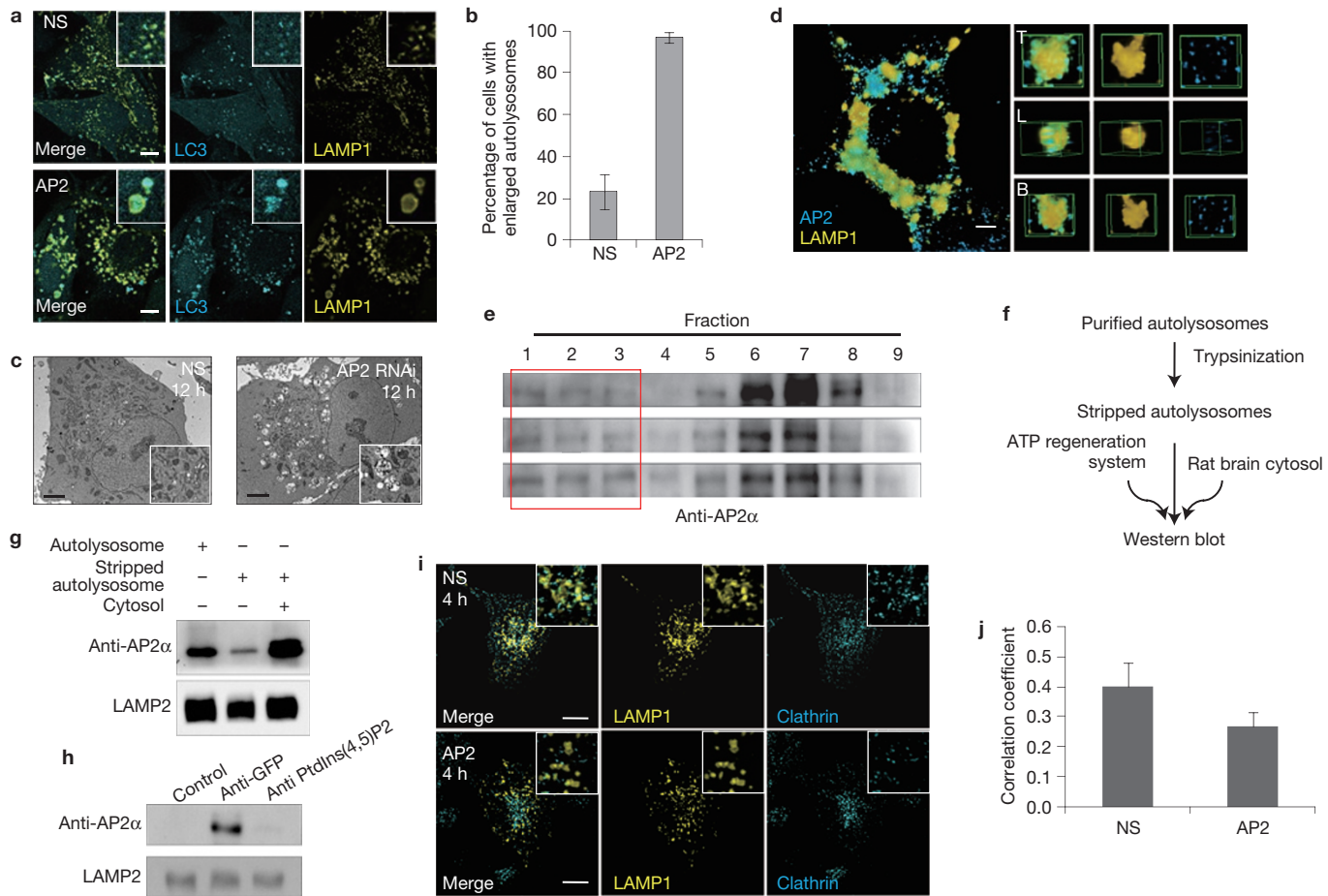


**Figure 5** AP2 is required for ALR. **(a)** NRK cells stably expressing CFP-LC3; LAMP1-YFP were transfected with nonspecific (NS)- or AP2-RNAi and starved for 12 h. Scale bars, 5  $\mu$ m. **(b)** Cells from **a** were assessed for enlarged autolysosomes in a blind fashion after starvation and quantified.  $n = 100$  cells from three independent experiments. Error bars indicate the s.d. **(c)** Representative TEM micrographs of non-specific- or AP2-RNAi-transfected NRK cells after 12 h of serum starvation. Scale bars, 5  $\mu$ m. **(d)** NRK cells were starved for 4 h, stained with antibodies against AP2 and LAMP1, and then analysed by 3D-SIM. Scale bar, 5  $\mu$ m. The right panels show enlarged regions of interest from the left panel: T, top view; L, lateral view; B, bottom view. **(e)** Fractions from Fig. 2f were analysed by western blotting with an antibody against AP2 $\alpha$ . The outline indicates the LAMP2-positive fraction. **(f)** Outline of the AP2 recruitment

recruited to autolysosomes through PtdIns(4,5)P<sub>2</sub>, we designed an *in vitro* AP2-autolysosome binding assay (Fig. 5f). In brief, the purified autolysosomes were trypsinized to remove surface proteins, and the stripped autolysosomes were then incubated with rat brain cytosol and an ATP regeneration system. We found that trypsinization removed the most of the AP2 from autolysosomes, and incubation of the trypsinized autolysosomes with rat brain cytosol caused recruitment of large amounts of AP2 (Fig. 5g). Pre-incubating the trypsinized autolysosomes with antibody against PtdIns(4,5)P<sub>2</sub> largely blocked the recruitment of AP2 (Fig. 5h). Thus, we conclude that AP2 is recruited to autolysosomes by PtdIns(4,5)P<sub>2</sub>. Not surprisingly, we also found that AP2 knockdown caused a reduced amount of co-localization of clathrin and autolysosomes (Fig. 5i,j). These data, together with the established role of AP2 in clathrin-coated vesicle formation, suggested that AP2

assay. **(g)** Purified autolysosomes were treated with trypsin, incubated with rat brain cytosol, washed and then analysed by western blot with antibodies against AP2 $\alpha$  and LAMP2. **(h)** Stripped autolysosomes were pretreated with GFP or PtdIns(4,5)P<sub>2</sub> antibody and then incubated with rat brain cytosol. Autolysosomes were washed and then analysed by western blotting with antibodies against AP2 $\alpha$  and LAMP2. **(i)** NRK cell lines stably expressing LAMP1-Cherry;clathrin-GFP were transfected with nonspecific- or AP2-RNAi and starved for 12 h. Scale bar, 5  $\mu$ m. The insets in **a**, **c** and **i** represent enlarged regions of interest. **(j)** Cells from **i** were analysed for the Pearson's co-localization coefficient ( $R(r)$ ) by Olympus Fluoview.  $n = 30$  cells from three independent experiments. Error bars indicate the s.d. Uncropped images of blots are shown in Supplementary Fig. S6.

probably directly regulates ALR by linking clathrin to PtdIns(4,5)P<sub>2</sub>. Beside its role in linking clathrin to PtdIns(4,5)P<sub>2</sub>, AP2 may also play a role in cargo sorting during ALR, which remains to be investigated.

#### AP4 is required for ALR

Clathrin binds its cargo proteins through different adaptor proteins<sup>24,25</sup>. We screened genes for other known clathrin adaptor proteins, including AP1, AP4, and Epsin R. We found that knockdown of AP4 blocks ALR and leads to the accumulation of enlarged autolysomes after 12 h of starvation (Fig. 6a–c and Supplementary Fig. S2).

Next, we measured the amount of AP4 on purified lysosomes/autolysosomes. Before starvation, only a small amount of AP4 is present on lysosomes, but the level of AP4 on autolysosomes markedly increased shortly after autolysosome formation and during

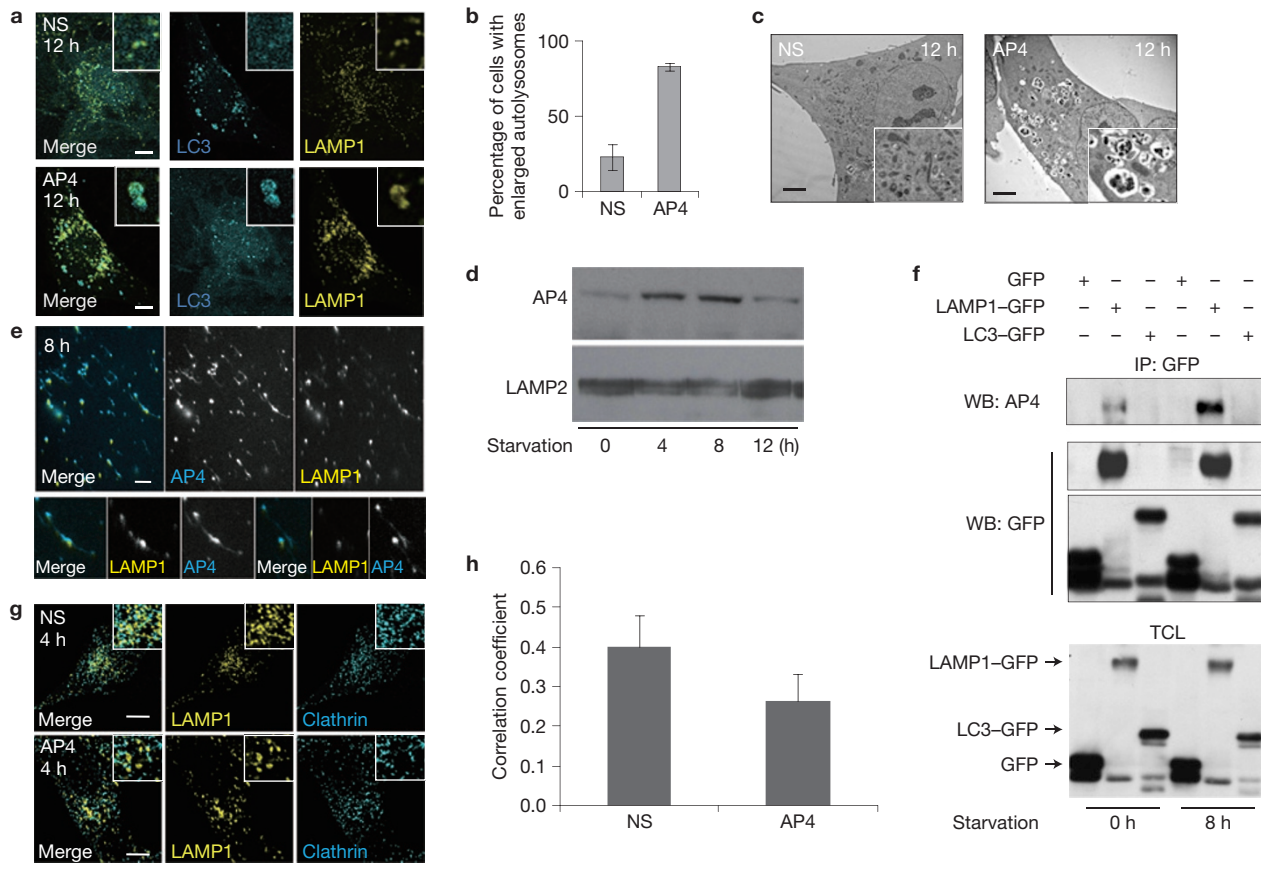


**Figure 6** AP4 is required for ALR. **(a)** NRK cells stably expressing CFP-LC3; LAMP1-YFP were transfected with nonspecific (NS)- or AP4-RNAi and starved for 12 h. Scale bars, 5 μm. **(b)** Cells from **a** were assessed for enlarged autolysosomes in a blind fashion after starvation and quantified.  $n = 100$  cells from three independent experiments. Error bars indicate the s.d. **(c)** Representative TEM micrographs of nonspecific- or AP4-RNAi-transfected NRK cells after 12 h of serum starvation. Scale bars, 5 μm. **(d)** NRK cells were starved for 0, 4, 8 or 12 h, and isolated lysosomes/autolysosome were analysed by western blotting using antibodies against AP4 or LAMP2. **(e)** Purified reformation tubules were stained with antibodies against AP4 and LAMP1. Scale bar, 2 μm. The bottom row shows enlarged regions of

interest from the top panel. **(f)** NRK cells were transfected with GFP and LAMP1-GFP. At 20 h after transfection, cells were starved for 0 or 8 h, and then collected and analysed by immunoprecipitation (IP) and western blotting (WB) of proteins as indicated, using stably expressed LAMP1-GFP as bait. TCL, total cell lysate. The insets in **a**, **c** and **g** represent enlarged regions of interest. **(g)** NRK cell lines stably expressing LAMP1-Cherry; clathrin-GFP were transfected with nonspecific- or AP4-RNAi and starved for 12 h. Scale bars, 5 μm. **(h)** Cells from **g** were analysed for the Pearson's co-localization coefficient ( $R(r)$ ) by Olympus Fluoview.  $n = 30$  cells from three independent experiments. Error bars indicate the s.d. Uncropped images of blots are shown in Supplementary Fig. S6.

ALR (Fig. 6d). Staining purified reformation tubules with antibodies against AP4 and LAMP1 revealed the presence of AP4 on reformation tubules (Fig. 6e).

Next, we investigated whether AP4 interacts with autolysosomal proteins. We could not detect any interaction between AP4 and LC3. However, we found that whereas there is little interaction between AP4 and LAMP1 before starvation, the level of interaction between AP4 and LAMP1 increased after 8 h of starvation (Fig. 6f). We also observed that the amount of co-localization of clathrin and autolysosomes is slightly reduced in AP4 knockdown cells, indicating that the interaction between AP4 and LAMP1 may play a role in the recruitment of clathrin to autolysosomes (Fig. 6g,h). Together, these data indicate that on starvation, AP4 plays a role in ALR by interacting with lysosomal proteins on autolysosomes and reformation tubules, which may in turn affect recruitment of clathrin to autolysosomes. We speculate that AP4 may play a role in the sorting of lysosomal cargo into reformation tubules.

### Clathrin and its associated proteins directly mediate bud formation on autolysosomes

So far, the evidence suggests that clathrin, AP2, AP4 and PIP(4,5)P<sub>2</sub> may directly mediate ALR. To investigate how clathrin may contribute to ALR, we set up an *in vitro* clathrin-binding and membrane deformation assay modified from a previous protocol<sup>26</sup>. In brief, autolysosomes were purified and treated with trypsin to remove surface proteins. These stripped autolysosomes were added to a reaction mixture containing rat brain cytosol, an ATP regeneration system and a buffer system. The autolysosomes were then washed and analysed by western blotting for association of clathrin and by scanning electron microscopy for clathrin-mediated membrane deformation. We found that a brief trypsin treatment effectively removed clathrin from purified autolysosomes while leaving intact most of the LAMP2, a highly glycosylated lysosomal membrane protein. Adding stripped autolysosomes to the reaction mix caused recruitment of clathrin to autolysosomes (Fig. 7a). Using scanning electron microscopy, we

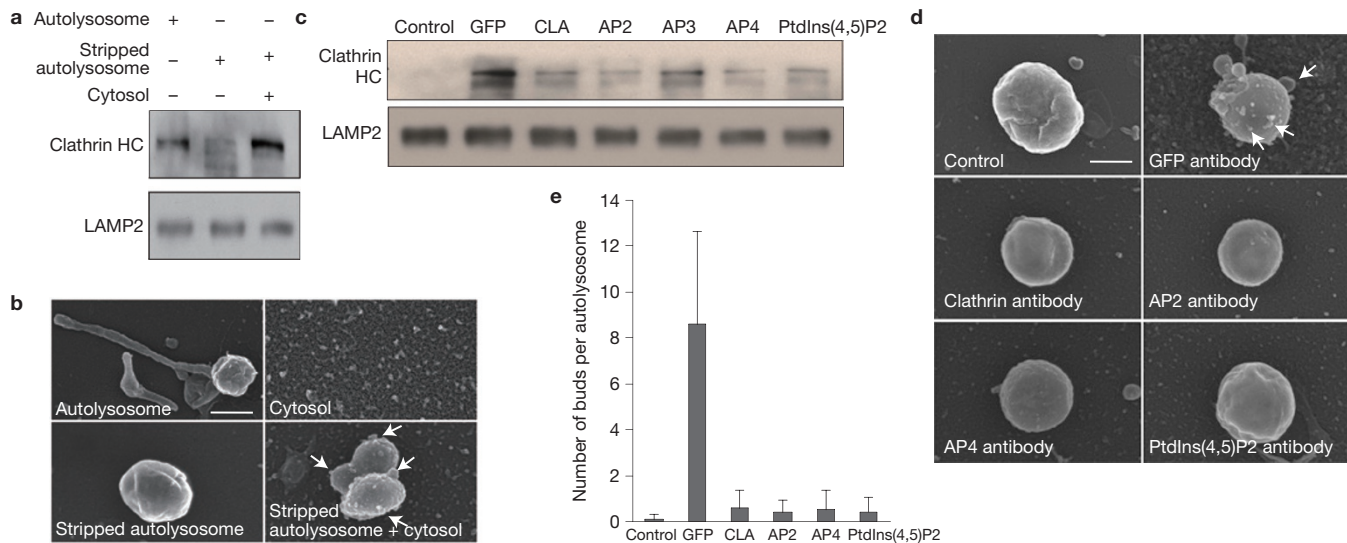


**Figure 7** Clathrin mediates autolysosome membrane budding. **(a)** Purified autolysosomes were treated with trypsin. The trypsin-treated (stripped) autolysosomes were incubated with rat brain cytosol and reaction mixture, and then analysed by western blotting. HC, heavy chain. **(b)** Scanning electron micrographs of purified autolysosomes, rat brain cytosol, trypsin-treated purified autolysosomes and trypsin-treated purified autolysosomes after the membrane budding assay. Scale bar, 250 nm. The arrows indicate buds. **(c)** Trypsin-treated autolysosomes were incubated

observed that the purified autolysosomes were spherical or tubular; however, after trypsin treatment, most became spherical with a smooth surface. Adding stripped autolysosomes to the reaction mix resulted in the formation of buds of different sizes (Fig. 7b). These data indicated that clathrin can be recruited to autolysosomes.

Next, we used the same *in vitro* assay to investigate whether autolysosome budding is directly mediated by clathrin and its associated proteins or PtdIns(4,5)P<sub>2</sub>. We added antibodies against these molecules to the reaction mix and investigated whether budding was inhibited. We found that antibodies against clathrin, AP2, AP4 and PtdIns(4,5)P<sub>2</sub> largely blocked the recruitment of clathrin to autolysosomes, whereas an antibody against AP3 had little or no effect (Fig. 7c). Scanning electron microscopy analysis confirmed that bud formation was largely inhibited by antibodies against clathrin, AP2, AP4 and PtdIns(4,5)P<sub>2</sub> (Fig. 7d,e). From these data, we conclude that clathrin, AP2, AP4 and PtdIns(4,5)P<sub>2</sub> directly mediate budding of autolysosomes. As knocking down all of the corresponding genes can block ALR, we speculated that clathrin-mediated autolysosome budding is required for extrusion of reformation tubules. We speculated that clathrin-mediated budding also occurs on reformation tubules and is required for fission of proto-lysosomes.

## DISCUSSION

Recently we reported the discovery of ALR, a cellular process that recycles lysosomal components from autolysosomes at the termination of autophagy. In this manuscript, we report the discovery of a clathrin-based mechanism that regulates the extrusion of reformation tubules, cargo sorting, PI(4)P to PtdIns(4,5)P<sub>2</sub> conversion and proto-lysosome budding. These data have enabled us to assemble a working model for the molecular and cellular events of ALR (Supplementary Fig. S3).

with rat brain cytosol and reaction mixture in the presence of antibodies against GFP, clathrin, AP2, AP3, AP4 and PtdIns(4,5)P<sub>2</sub>, and then analysed by western blotting. **(d)** Reactions from **c** were visualized by scanning electron microscopy. Scale bar, 250 nm. Arrow indicates bud. **(e)** Samples from **d** were quantified for the number of buds on each autolysosome. Error bars represent s.d. *n* = 50 autolysomes from three independent experiments. Uncropped images of blots are shown in Supplementary Fig. S6.

In this model, ALR is initiated by the conversion of autolysome-localized PI(4)P to PtdIns(4,5)P<sub>2</sub> by PIP5K1B. The generation of PtdIns(4,5)P<sub>2</sub> leads to recruitment of clathrin through its adaptor AP2 to PtdIns(4,5)P<sub>2</sub>-enriched microdomains of autolysosomes. Lysosomal membrane proteins are selectively enriched on these microdomains through direct interactions with AP4. Binding of clathrin to the relatively flat autolysosome surface leads to an increase in membrane curvature and initiation of the budding process, which then proceeds to tubule formation. Next, PIP5K1A, situated on the reformation tubules, generates PtdIns(4,5)P<sub>2</sub> on the reformation tubules. The generation of PtdIns(4,5)P<sub>2</sub> triggers the second round of clathrin recruitment on the reformation tubules, leading to the pinching off of proto-lysosomes. We stress that our working model for ALR is merely an outline for the process, and is most likely to be incomplete, as many more proteins probably remain to be discovered. Nevertheless, we believe that our model provides a molecular framework for understanding the cellular events of ALR. On the basis of our model, we can divide ALR into four steps, including PtdIns(4,5)P<sub>2</sub> generation, tubule initiation, tubule extension and proto-lysosome budding. This framework will be helpful to design further experiments to probe the molecular machinery of ALR.

Our screening strategy also identified AP3 and ASAP1 as regulators of ALR (Supplementary Fig. S4). Although at present we do not understand the exact role of these molecules in ALR, the fact that knocking down AP3 and ASAP1 changes the clathrin localization pattern and reduces clathrin recruitment to autolysosomes further supports the central role of clathrin in ALR.

Our data indicate that clathrin probably has two sites of action in ALR, one on the main body of autolysosomes, where it is required for the generation of reformation tubules, and the other on the tubules

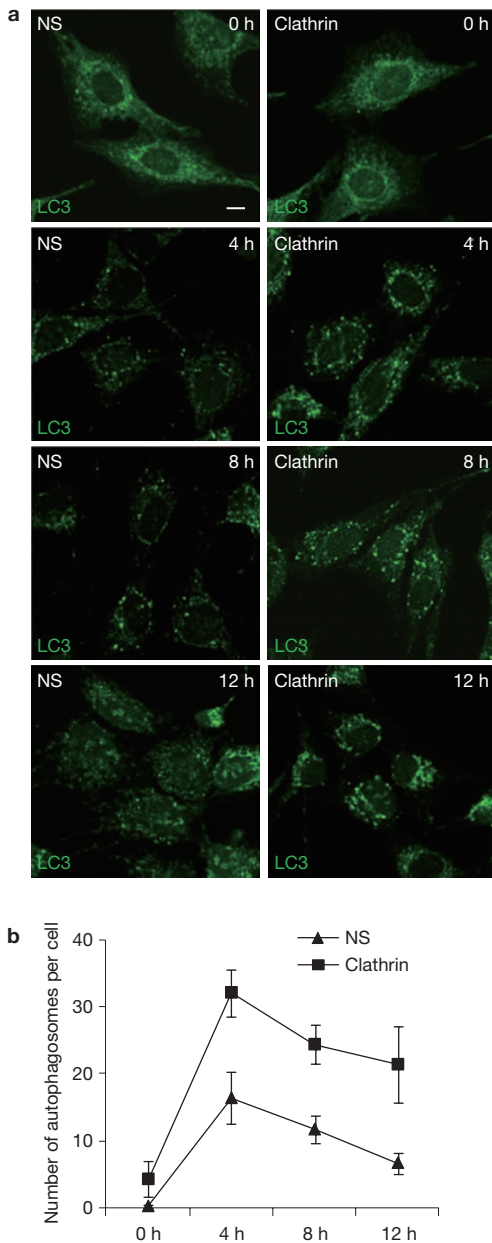


**Figure 8** Starvation induces LC3 puncta formation in clathrin knockdown cells. **(a)** NRK cells were transfected with nonspecific (NS)- or *Cltc* (clathrin heavy chain)-RNAi and starved for 0, 4, 8 or 12 h. Scale bar, 5 mm. Cells were stained with antibodies against LC3. **(b)** Cells from **a** were assessed for LC3 puncta in a blind fashion after starvation and quantified.  $n = 100$  cells from three independent experiments. Error bars indicate the s.d.

themselves, where it is required for the budding of proto-lysosomes. The role of clathrin in retromer-mediated early endosome retrograde sorting provides some clues<sup>12,27</sup> about how clathrin mediates the formation of reformation tubules. In this process, clathrin is required for cargo sorting and for the initial curvature of the endosome surface. Once the curvature is established, the retromer complex then causes tubulation. In this study, we observed that clathrin mediates bud formation on the surface of autolysosomes *in vitro*, which reflects the marked curvature change caused by clathrin. We also found that AP4 can bind to LAMP1 but not LC3; thus, despite a lack of direct

experimental evidence, we can speculate that the membrane curvature and cargo sorting caused by clathrin and its associated proteins are required for the initiation of tubulation through a sequence of events similar to endosome tubulation.

It is well established that clathrin is required for autophagosome formation<sup>28</sup>. However, we find that autophagosome formation is largely normal under our experimental condition (Fig. 8). One very likely explanation for this discrepancy is that clathrin plays a role in both autophagosome formation and ALR. As indicated previously<sup>28</sup>, the *Cltc* knockdown efficiency needs to be extremely high for it to affect autophagosome formation. For that reason, the authors of this previous study developed a new RNAi transfection protocol to achieve the highest possible knockdown efficiency. In our case, *Cltc* knockdown efficiency is moderate. It is therefore possible that moderate *Cltc* knockdown efficiency allows for autophagosome formation and progression to the autolysosome stage; whereas a highly effective *Cltc* knockdown blocks the formation of autophagosomes.

There are three isoforms of PIP5K1: A, B and  $\gamma$ . The  $\gamma$  isoform seemed to be the dominant isoform as PIP5K1A or B single- or double-knockout mice can survive to adulthood<sup>29</sup>. The fact that different PIP5K isoform knockout mice have different phenotypes indicates that the three isoforms may have different action sites and thus play different physiological roles. In our study, we found that PIP5K1A and PIP5K1B are both required for ALR, but they play different roles. We noticed that both PIP5K1A and PIP5K1B are present on autolysosomes whereas PIP5K1A is the main PI(4)P kinase present on reformation tubules. On the basis of this observation, we can speculate that the different phenotypes caused by *PIP5K1A* and *PIP5K1B* knockdown result from their preferential association with autolysosomes or reformation tubules at different stages of ALR. A more in-depth investigation is required to address the molecular mechanisms underlying their association and dissociation from autolysosomes. □

## METHODS

Methods and any associated references are available in the online version of the paper.

*Note:* Supplementary Information is available in the online version of the paper

## ACKNOWLEDGEMENTS

We are grateful to Olympus China, Nikon Instruments (Shanghai) and the Tsinghua Cell Biology Core Facility for providing technical support, and to Q. Dong, Y. Li and L. Huang for assistance with microscopy, TEM and image processing. We thank J.-J. Liu for helpful discussions and J. Lippincott-Schwartz and J. Bonifacino (Cell Biology and Metabolism Branch, National Institute of Child Health and Human Development, Bethesda, USA) for constructs and antibodies. This research was supported by 973 Program grants 2010CB833704 and 2011CB910100, National Science Foundation grants 31030043 and 30971484, and Tsinghua University grants 2010THZ0 and 2009THZ03071 to L.Y., and NSFC grant 81030040, MOST grant 2008ZX09401—002, 2011CB809106 to J.X.

## AUTHOR CONTRIBUTIONS

L.Y. and Y.R. conceived and designed the experiments. J.X. designed SAMCell base screening and H.Z. manufactured the SAMCell chip. L.L. and S.C. carried out the mass spectrometric analysis. Y.R., M.L., Y.T. and Z.C. carried out screening. Y.R. carried out the functional study with help from M.L. L.M., Y.T., H.R. and C.Z. performed the FESEM in manuscript revision experiments. Y.L. carried out the embedding and ultrathin sectioning for TEM experiments. W.D. carried out the *in vitro* staining experiments. L.Y. and Y.R. wrote the manuscript.

## COMPETING FINANCIAL INTERESTS

The authors declare no competing financial interests.

Published online at [www.nature.com/doifinder/10.1038/ncb2557](http://www.nature.com/doifinder/10.1038/ncb2557)

Reprints and permissions information is available online at [www.nature.com/reprints](http://www.nature.com/reprints)

1. Klionsky, D. J. Autophagy: from phenomenology to molecular understanding in less than a decade. *Nat. Rev. Mol. Cell Biol.* **8**, 931–937 (2007).
2. Mizushima, N. Autophagy: process and function. *Genes Dev.* **21**, 2861–2873 (2007).
3. Kraft, C. & Martens, S. Mechanisms and regulation of autophagosome formation. *Curr. Opin. Cell Biol.* <http://dx.doi.org/10.1016/j.ceb.2012.05.001> (2012).
4. Klionsky, D. J. & Emr, S. D. Autophagy as a regulated pathway of cellular degradation. *Science* **290**, 1717–1721 (2000).
5. Yu, L. *et al.* Termination of autophagy and reformation of lysosomes regulated by mTOR. *Nature* **465**, 942–946 (2010).
6. Rong, Y. *et al.* Spinster is required for autophagic lysosome reformation and mTOR reactivation following starvation. *Proc. Natl Acad. Sci. USA* **108**, 7826 (2011).
7. Zhang, H. *et al.* Genome-wide functional screening of miR-23b as a pleiotropic modulator suppressing cancer metastasis. *Nat. Commun.* **2**, 554 (2011).
8. Pawlowski, N. Dynamin self-assembly and the vesicle scission mechanism: how dynamin oligomers cleave the membrane neck of clathrin-coated pits during endocytosis. *Bioessays* **32**, 1033–1039 (2010).
9. Kirchhausen, T. Clathrin. *Annu. Rev. Biochem.* **69**, 699–727 (2000).
10. Mettlen, M., Loerke, D., Yarar, D., Danuser, G. & Schmid, S. L. Cargo- and adaptor-specific mechanisms regulate clathrin-mediated endocytosis. *J. Cell Biol.* **188**, 919–933 (2010).
11. Raiborg, C. *et al.* Hrs sorts ubiquitinated proteins into clathrin-coated microdomains of early endosomes. *Nat. Cell Biol.* **4**, 394–398 (2002).
12. Popoff, V. *et al.* The retromer complex and clathrin define an early endosomal retrograde exit site. *J. Cell Sci.* **120**, 2022–2031 (2007).
13. Shi, A. *et al.* Regulation of endosomal clathrin and retromer-mediated endosome to Golgi retrograde transport by the J-domain protein RME-8. *EMBO J.* **28**, 3290–3302 (2009).
14. Di Paolo, G. & De Camilli, P. Phosphoinositides in cell regulation and membrane dynamics. *Nature* **443**, 651–657 (2006).
15. Divecha, N. & Irvine, R. F. Phospholipid signaling. *Cell* **80**, 269–278 (1995).
16. Funakoshi, Y., Hasegawa, H. & Kanaho, Y. Activation mechanisms of PIP5K isozymes by the small GTPase ARF6. *Adv. Enzyme Regul.* **50**, 72–80 (2010).
17. van den Bout, I. & Divecha, N. PIP5K-driven PtdIns(4,5)P<sub>2</sub> synthesis: regulation and cellular functions. *J. Cell Sci.* **122**, 3837–3850 (2009).
18. Boronenkov, I. V. & Anderson, R. A. The sequence of phosphatidylinositol-4-phosphate 5-kinase defines a novel family of lipid kinases. *J. Biol. Chem.* **270**, 2881–2884 (1995).
19. Rohde, G., Wenzel, D. & Haucke, V. A phosphatidylinositol (4,5)-bisphosphate binding site within mu2-adaptin regulates clathrin-mediated endocytosis. *J. Cell Biol.* **158**, 209–214 (2002).
20. Levine, T. P. & Munro, S. Targeting of Golgi-specific pleckstrin homology domains involves both PtdIns 4-kinase-dependent and -independent components. *Curr. Biol.* **12**, 695–704 (2002).
21. Lehto, M. & Olkkonen, V. M. The OSBP-related proteins: a novel protein family involved in vesicle transport, cellular lipid metabolism, and cell signalling. *Biochim. Biophys. Acta* **1631**, 1–11 (2003).
22. Ford, M. G. J. *et al.* Simultaneous binding of PtdIns(4,5)P<sub>2</sub> and clathrin by AP180 in the nucleation of clathrin lattices on membranes. *Science* **291**, 1051–1055 (2001).
23. Smythe, E., Carter, L. L. & Schmid, S. L. Cytosol- and clathrin-dependent stimulation of endocytosis *in vitro* by purified adaptors. *J. Cell Biol.* **119**, 1163–1171 (1992).
24. McNiven, M. A. & Thompson, H. M. Vesicle formation at the plasma membrane and trans-golgi network: the same but different. *Science* **313**, 1591–1594 (2006).
25. Schmid, S. L. Clathrin-coated vesicle formation and protein sorting: an integrated process. *Annu. Rev. Biochem.* **66**, 511–548 (1997).
26. Traub, L. M. *et al.* AP-2-containing clathrin coats assemble on mature lysosomes. *J. Cell Biol.* **135**, 1801–1814 (1996).
27. Popoff, V. *et al.* Analysis of articulation between clathrin and retromer in retrograde sorting on early endosomes. *Traffic* **10**, 1868–1880 (2009).
28. Ravikumar, B., Moreau, K., Jahreiss, L., Puri, C. & Rubinsztein, D. C. Plasma membrane contributes to the formation of pre-autophagosomal structures. *Nat. Cell Biol.* **12**, 747–757 (2011).
29. Volpicelli-Daley, L. A. *et al.* Phosphatidylinositol-4-phosphate 5-kinases and phosphatidylinositol 4,5-bisphosphate synthesis in the brain. *J. Biol. Chem.* **285** (2010).

## METHODS

**Reagents and antibodies.** Anti-LAMP1 (L1418) antibody, anti-PIP5K1B (K0767) antibody and anti-ASAP1 (A4102) antibody were from Sigma-Aldrich. Anti-GFP (11814460001) antibody was from Roche. Anti-clathrin heavy chain X22 antibody and anti-AP-2 alpha subunit (MA3-061) antibody were from Thermo Fisher Scientific. Anti-PIP5K1A (15713-1-AP) antibody was from Proteintech Group; anti-LAMP1 (ADI-VAM-EN001) antibody was from Enzo Life Sciences. Anti-clathrin heavy chain (#2410) antibody was from Cell Signaling Technology. Anti-PI(4)P (Z-P004) and anti-PtdIns(4,5)P<sub>2</sub> (Z-G045) antibodies were from Echelon Biosciences. Anti-LC3 (PM046) and anti-LAMP2 (EP-6041) antibodies were from MBL. Anti-AP-4 epsilon subunit (612018) antibody was from BD Transduction Laboratories. The antibodies described above were used at dilutions of 1:1,000 (for immunoblotting) and 1:100 (for immunofluorescence microscopy and immunoprecipitation).

**Cell culture and transfection.** NRK cells were obtained from the American Type Culture Collection (ATCC) and cultured in DMEM (Life Technologies) medium supplemented with 10% FBS (5% CO<sub>2</sub>). Cells were transfected with 200 pmol RNAi or a total of 2 µg DNA through Amaxa nucleofection using solution T and program X-001. Cells were then cultured in growth medium for further analysis. For two rounds of transfection, cells were transfected with 200 pmol RNAi, and 72 h after transfection, cells were transfected again with 100 pmol RNAi and up to 2 µg DNA.

**Constructs.** CFP-Arf1, CFP-Arf1-Q71L, CFP-LC3 and LAMP-1-Cherry red constructs were provided by J. Lippincott-Schwartz (National Institutes of Health, USA). OSBP-PH was kindly provided by J. Liu (Institute of Genetics and Developmental Biology, Chinese Academy of Science, China). Clathrin-GFP was a gift from S. Shenfang (Tsinghua University, China).

**Mass spectrometric analysis.** Protein bands on SDS-PAGE gels were de-stained and in-gel digested with sequencing-grade trypsin (10 ng µl<sup>-1</sup> trypsin and 50 mM ammonium bicarbonate, at pH 8.0) overnight at 37 °C. Peptides were extracted with 5% formic acid/50% acetonitrile and 0.1% formic acid/75% acetonitrile sequentially and then concentrated to ~20 µl. The extracted peptides were separated using an analytical capillary column (50 µm × 10 cm) packed with 5 µm spherical C18 reversed-phase material (YMC). An Agilent 1100 series binary pump system (Agilent Technologies) was used to generate the following HPLC gradient: 0–5% B in 5 min, 5–40% B in 70 min, 40–100% B in 10 min (A, 0.2 M acetic acid in water; B, 0.2 M acetic acid/70% acetonitrile). The eluted peptides were sprayed into an LTQ mass spectrometer (Thermo Fisher Scientific) equipped with a nano-ESI ion source. The mass spectrometer was operated in data-dependent mode with one MS scan followed by five MS/MS scans for each cycle. Database searches were performed on an in-house Mascot server (Matrix Science) against the IPI (International Protein Index) rat protein database. Methionine oxidation was set as a variable modification.

**Fabrication of SAMCell.** Glass slides (2.2 cm × 2.2 cm) were washed with detergent and milliQ water. After drying, the slides were covered with 65 µl of 6% (w/v) poly (*N*-isopropylacrylamide) (Aldrich) dissolved in ethanol and stored for at least 12 h at room temperature. The slides were etched using a shadow mask by oxygen plasma for 3.5 min at 200 W power. The reverse transfection protocol has been described previously (Erfle, 2007). In brief, 3 µl of OptiMEM (Invitrogen) containing sucrose and Lipofectamine 2000 (Invitrogen) was transferred to each 200 µl tube and mixed thoroughly. Then, 1 µl short interfering RNA (siRNA; 100 µM) was added to each tube and the mixture was incubated for 20 min at room temperature. Finally, 7.25 µl of a 0.2% (w/v) gelatin (Sigma, Type B) solution was added to each tube and mixed thoroughly. After ultraviolet sterilization, the reverse transfection reagent was printed on the chip using a nanodispenser (Phoenix, Art Robbins Instruments). Next, the slides were fixed in a 6-well plate with melted wax. About 3 ml of medium at 37 °C containing 5 × 10<sup>5</sup> cells was transferred in each well. About 24–48 h later, the dishes were moved to room temperature for 5 min and washed three times with PBS to ensure total removal of the polymer. The cell microarray was then recorded using a microscope system.

**Live-cell imaging.** Transfected cells were re-plated in Lab-Tek chambered coverglass (NUNC) the night before imaging, and cells were maintained at 37 °C with 5% CO<sub>2</sub> in a PeCon open chamber (PeCon, Erbach). Images were acquired using an Olympus FV-1000 confocal microscope.

**Cell fractionation.** Cell fractionation and lysosome isolation were performed with a lysosome isolation kit (Sigma-Aldrich) according to the manufacturer's manual.

**Staining.** Cells were washed with phosphate buffered saline (PBS), fixed in 2% paraformaldehyde for 10 min, and permeabilized in 0.2% Triton X-100 for 5 min. Fixed cells were blocked with 10% FBS in PBS for 30 min, stained with 10 µg ml<sup>-1</sup> of antibody in blocking buffer for 1 h, and washed with PBS three times. Cells were then stained with secondary antibody in PBS for 1 h and washed with PBS three times.

**3D-SIM.** NRK cells were plated on glass coverslips for 24 h and starved for 4 h. After immunostaining, 3D-images were acquired on an N-SIM using a ×100 oil-immersion lens (numerical aperture 1.49) by Z-stack scanning at 0.2 or 0.4 µm intervals. Laser lines at 488 and 561 nm were used for excitation using Nikon's N-SIM microscopy system, which can achieve a resolution of 100 nm along the x-y axis and 300 nm along the z axis. The instrument resolution is verified by 100 nm fluorescent spheres according to the Nikon procedure after installation.

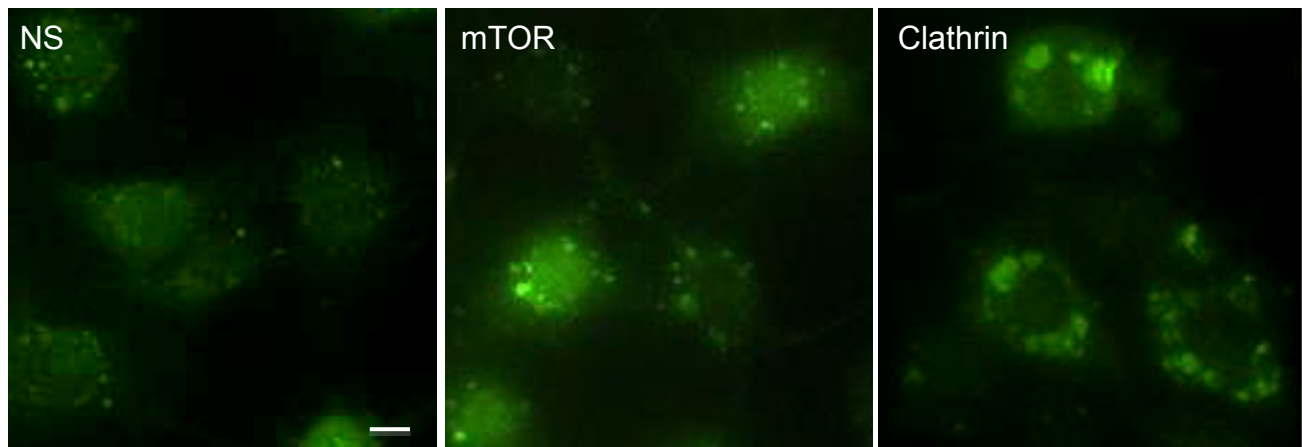
**Electron microscopy.** Cells were fixed in 3% glutaraldehyde in 0.1 M MOPS buffer (pH 7.0) for 8 h at room temperature, and then 3% glutaraldehyde/1% paraformaldehyde in 0.1 M MOPS buffer (pH 7.0) for 16 h at 4 °C. They were then post-fixed in 1% osmium tetroxide for 1 h, and embedded in Spurr's resin, sectioned, doubly stained with uranyl acetate and lead citrate, and analysed using a Zeiss EM 10 transmission electron microscope.

**Rat brain cytosol preparation.** Rat brains were homogenized in breaking buffer (25 mM HEPES-KOH, at pH 7.4, 250 mM sucrose and 2 mM EDTA) in the presence of a protease inhibitor cocktail. The lysate was centrifuged at 160,000 $\times$ g for 1 h and the resulting supernatant was desalting on PD-10 columns equilibrated in 25 mM HEPES-KOH, at pH 7.0, 250 mM sucrose, 125 mM potassium acetate, 5 mM magnesium acetate and 1 mM dithiothreitol.

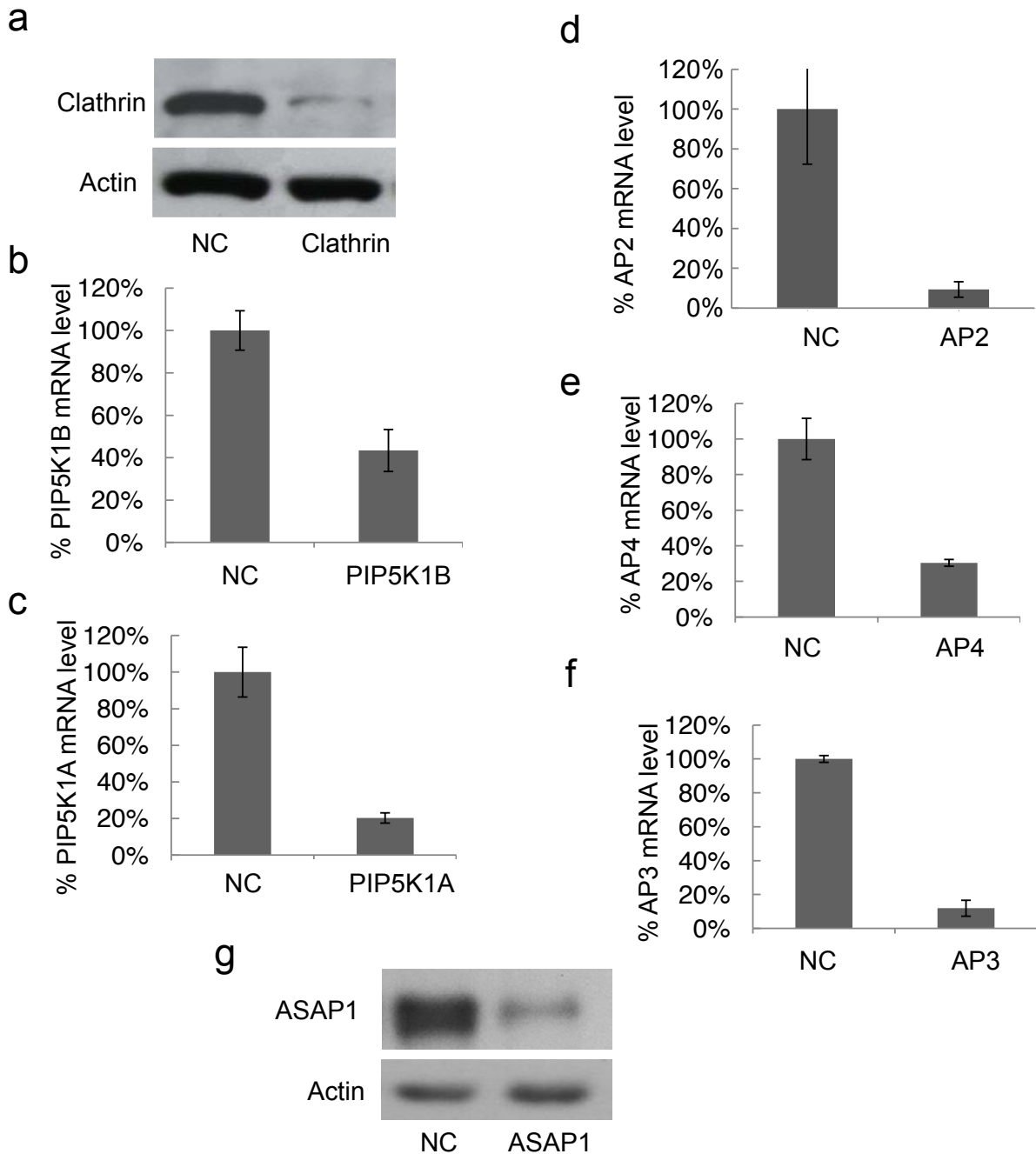
**In vitro membrane-binding assay.** Lysosomes, prepared in the absence of protease inhibitors, were treated with trypsin. Aliquots of the pretreated lysosomes were then added to binding reactions containing gel-filtered rat brain cytosol that was pre-incubated with antibodies of anti-GFP (400 µg ml<sup>-1</sup>), anti-clathrin heavy chain (400 µg ml<sup>-1</sup>), anti-AP2α (200 µg ml<sup>-1</sup>), anti-AP3δ (25 µg ml<sup>-1</sup>), anti-AP4ε (25 µg ml<sup>-1</sup>) or anti-PtdIns(4,5)P<sub>2</sub> (100 µg ml<sup>-1</sup>) as indicated at 4 °C for 1–2 h and the ATP regeneration system (4.6 IU ml<sup>-1</sup> creatine phosphokinase, 81 mM creatine phosphate and 2 mM ATP) was added last, after a 1 h incubation at 37 °C; reactions were terminated by chilling on ice. After centrifugation, the membrane-containing pellets were prepared for immunoblotting or field emission in lens scanning electron microscopy (FEISEM).

**FEISEM.** For FEISEM, lysosome and cytosol were incubated on glass chips at 37° for 1 h, and then fixed with 2% glutaraldehyde in PBS buffer at room temperature for 30 min. Then, the samples were rinsed and post-fixed with 1.0% OsO<sub>4</sub> in 0.1 M sodium cacodylate buffer at room temperature for 20 min. After dehydration in a graded series of ethanol (30%, 50%, 70%, 90%, 100%, 100%, 10 min each), the samples were transferred to Arkline for critical-point drying using highest-purity CO<sub>2</sub> in a Hitachi HCP-2 Critical Point Dryer. The samples were then coated with 4 nm gold in a Hitachi E-1045 ion sputter coater and viewed in a Hitachi scanning electron microscope S4800 at a 6 kV accelerating voltage.

**Statistical tests.** Statistical analysis was carried out on the data from independent experiments. The error bars in the figures represent s.d.; the n value is specified in the legends.

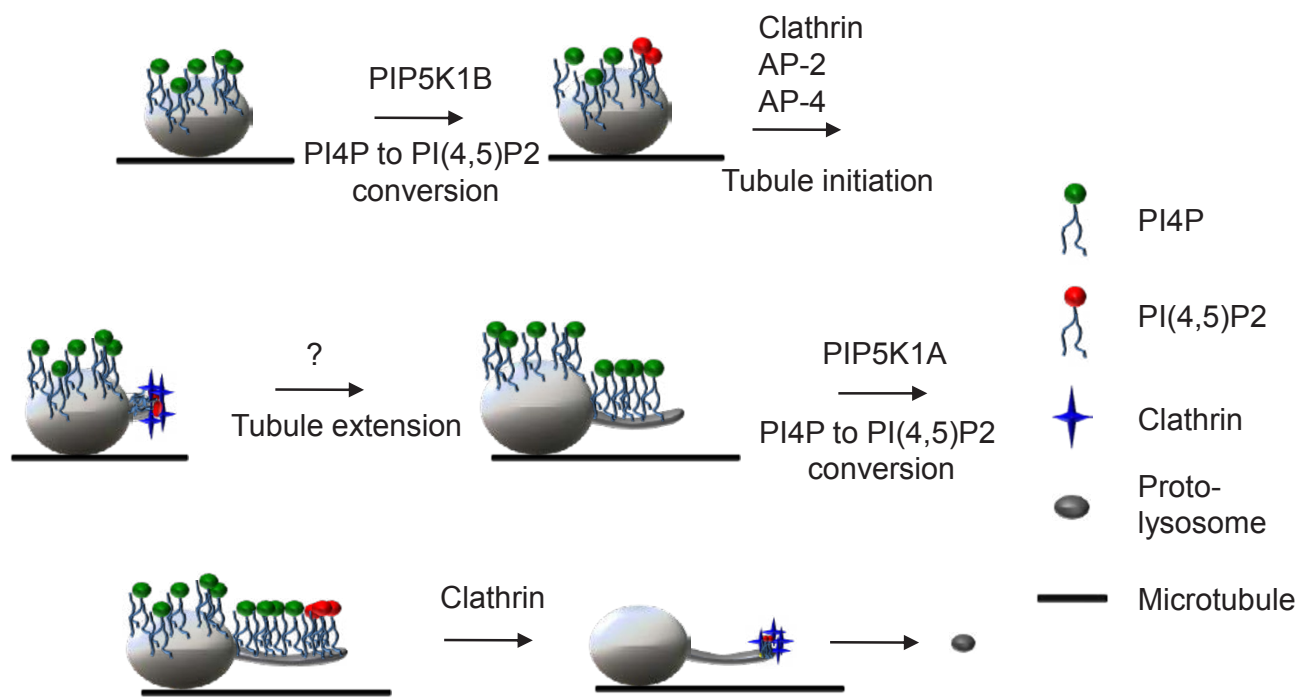


**Figure S1** Images that typify a positive (mTOR, clathrin) and negative (NS) screen result. Scale bar, 5  $\mu\text{m}$ .

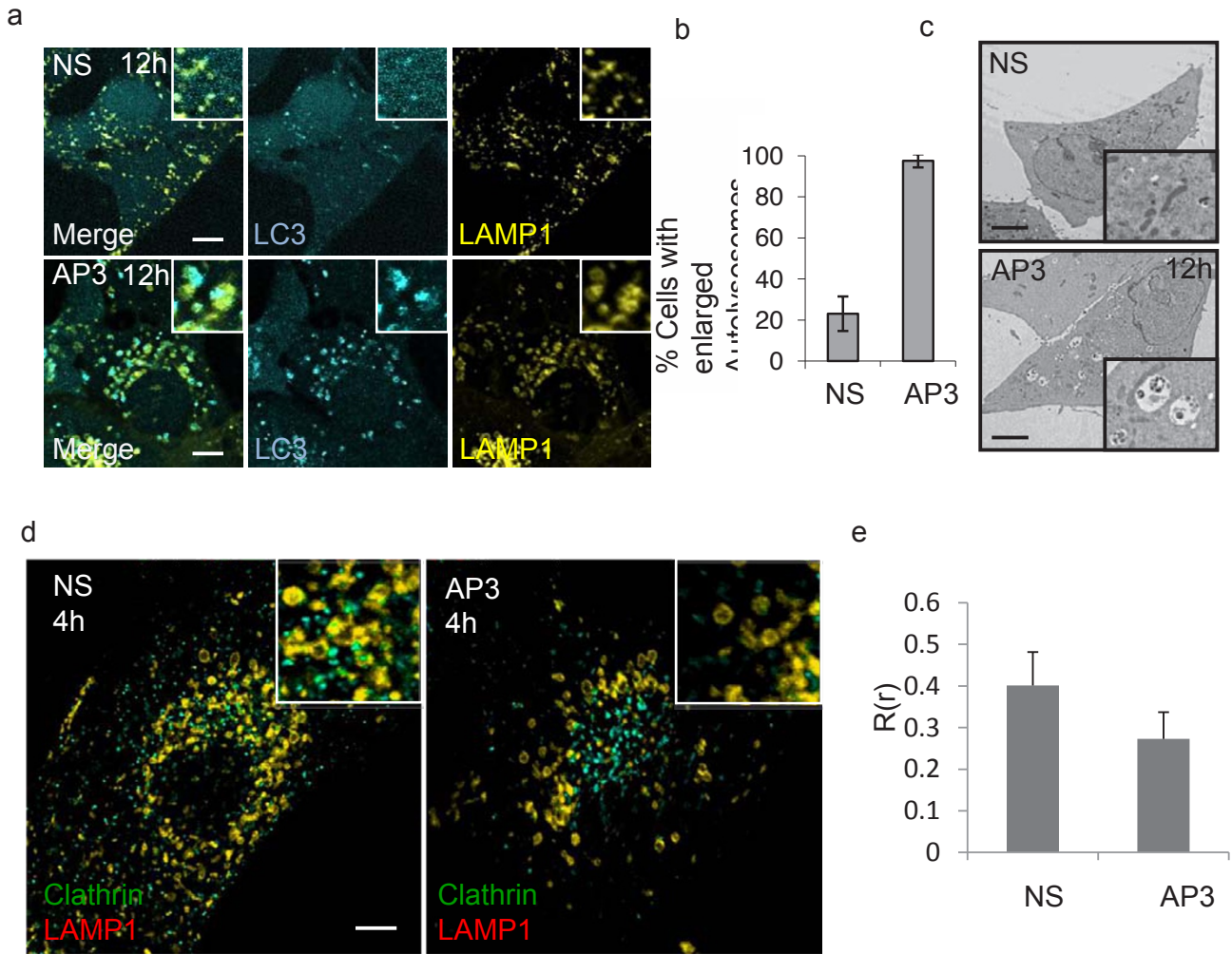


**Figure S2** RNAi knockdown efficiency. Cells were transfected with non-specific or RNAi against candidate genes. 60 hours after transfection, mRNA levels of candidate genes were measured by qPCR and protein levels were measured by western blot. qPCR was performed in triplicate and the data represent the mean  $\pm$  S.D (n=3).

## SUPPLEMENTARY INFORMATION



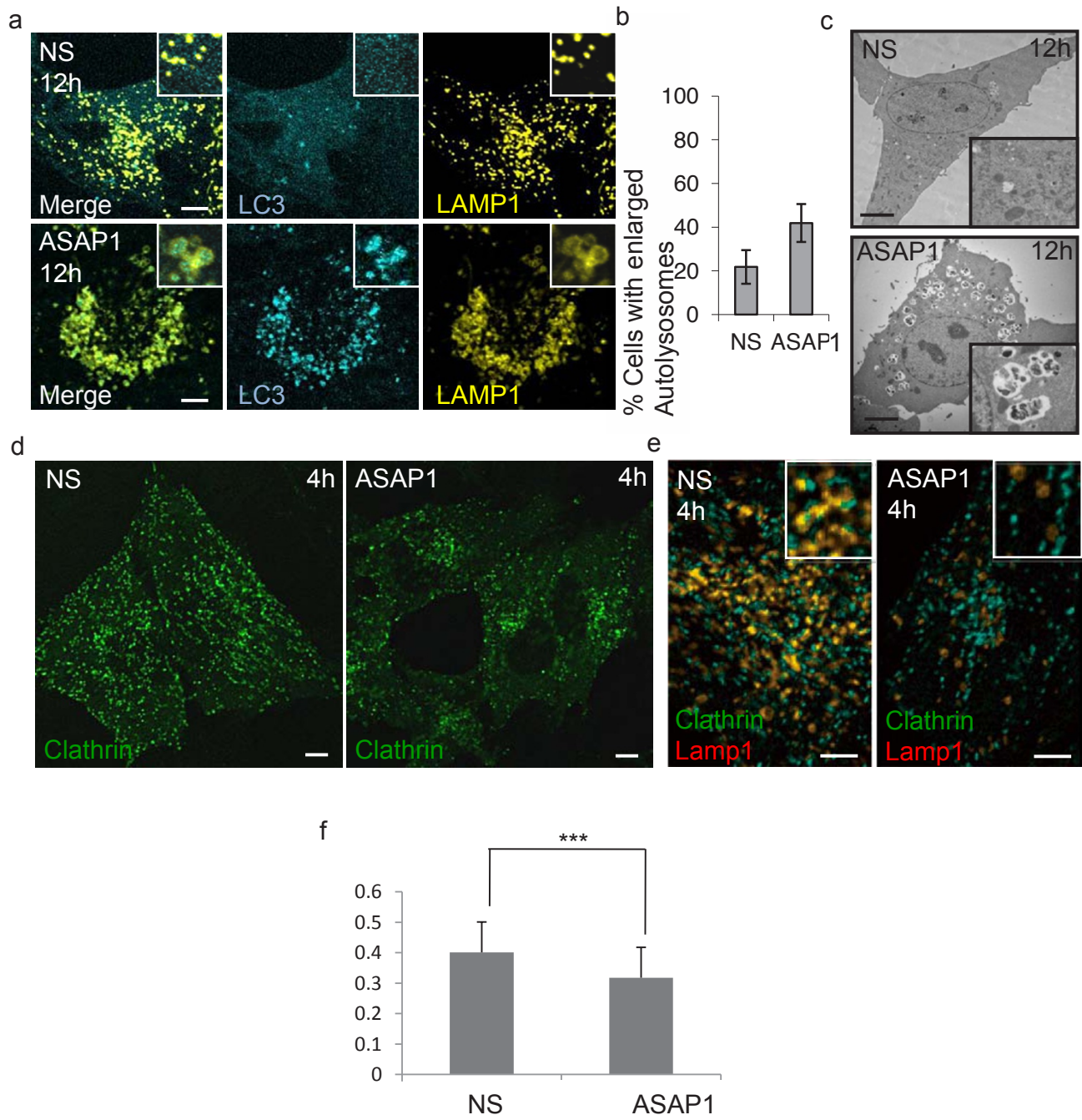
**Figure S3** Provisional model of the molecular regulation of ALR.



**Figure S4** (a) NRK-CFP-LC3; LAMP1-YFP stable cells were transfected with nonspecific (NS)- or AP3-RNAi and starved for 12 h. Scale bars, 5 mm. (b) Cells from (a) were assessed for enlarged autolysosomes in a blind fashion after starvation and quantified. One hundred cells were counted. Error bars indicate the standard deviation. (c) Representative transmission electron micrographs of nonspecific (NS) or AP3-RNAi-transfected NRK

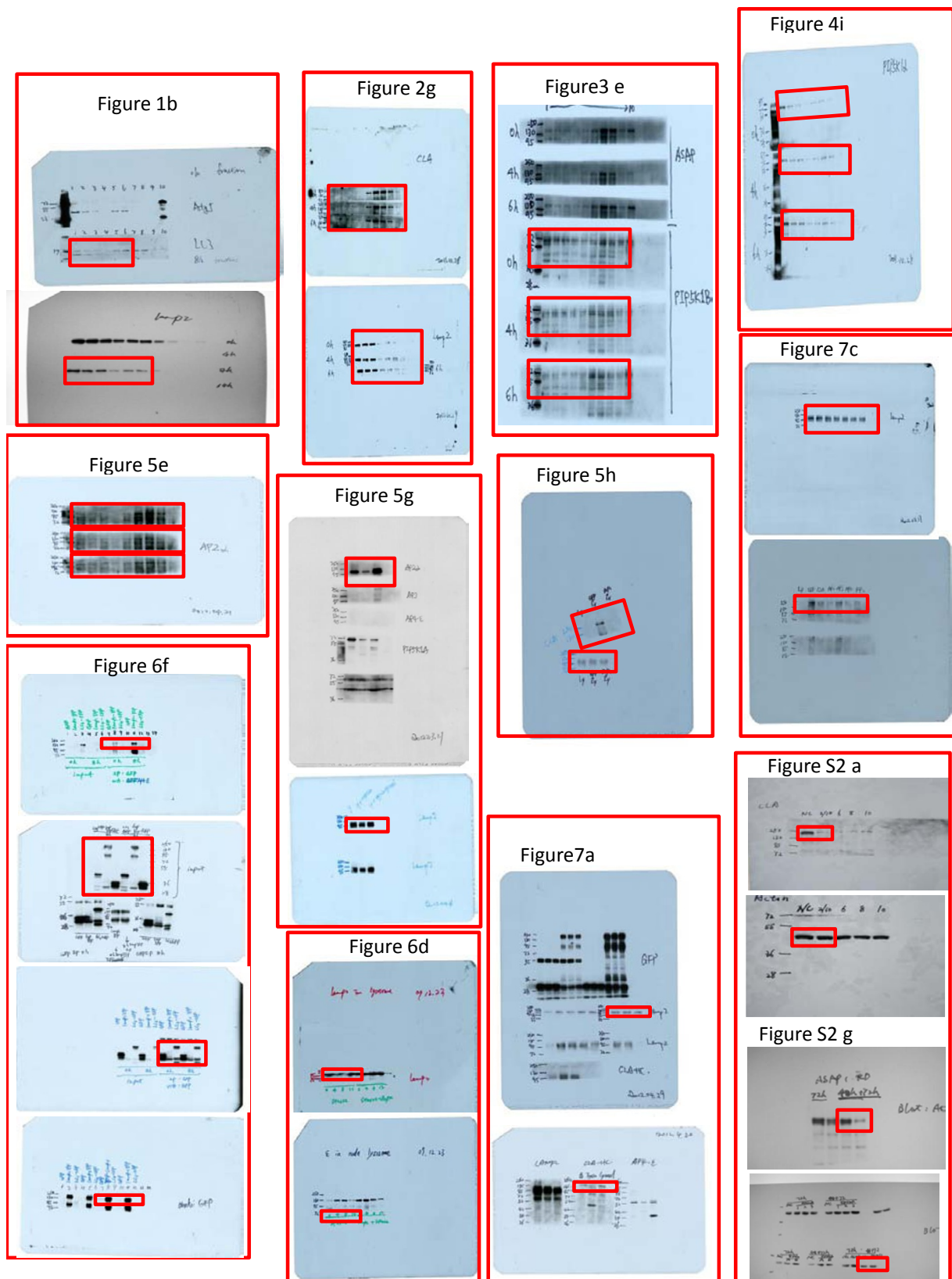
cells after 12 hours of serum starvation. Scale bars, 5 mm. (d) NRK-LAMP1-Cherry; clathrin-GFP stable cell lines were transfected with nonspecific (NS)- or AP3-RNAi and starved for 12 h. Scale bars, 5 mm. Co-localization of LAMP1 and clathrin was analyzed using Olympus Fluoview (e). n = 30 cells from 3 independent experiments. Error bars indicate the standard deviation.

## SUPPLEMENTARY INFORMATION



**Figure S5** ASAP1 regulates ALR. (a) NRK-CFP-LC3; LAMP1-YFP stable cells were transfected with nonspecific (NS)- or ASAP1-RNAi and starved for 12 h. Scale bars, 5 mm. (b) Cells from (a) were assessed for enlarged autolysosomes in a blind fashion after starvation and quantified. One hundred cells were counted. Error bars indicate the standard deviation. (c) Representative transmission electron micrographs of nonspecific (NS)- or

ASAP1-RNAi-transfected NRK cells after 12 hours of serum starvation. Scale bars, 5 mm. (d,e) NRK-LAMP1-Cherry; clathrin-GFP stable cell lines were transfected with nonspecific (NS)- or ASAP1-RNAi and starved for 12 h. Scale bars, 5 mm. Co-localization of LAMP1 and clathrin was analyzed using Olympus Fluoview (f). n = 30 cells from 3 independent experiments. Error bars indicate the standard deviation.

**Figure S6** Full scans of immuno-blots shown in Figs 1-7 and FigS1.

## SUPPLEMENTARY INFORMATION

### Supplemental Table Titles:

Table S1: LC-MS/MS Instrument methods and database search parameters.

Table S2: Proteins identified by proteomic analysis on purified reformation tubules.

Table S3: RNAi sequence of used in SAMCell screening.